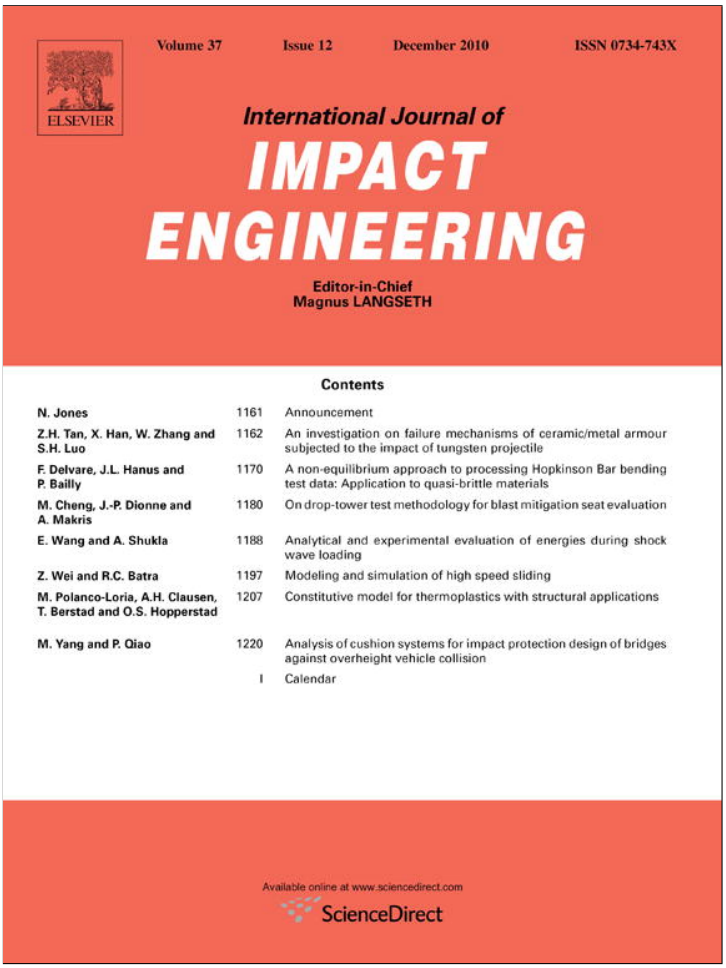
Volume 37 Issue 12 December 2010 ISSN 0734-743X

ELSEVIER

International Journal of
IMPACT ENGINEERING

Editor-in-Chief
Magnus LANGSETH

Contents

Available online at www.sciencedirect.com
ScienceDirect

International Journal of Impact Engineering 37 (2010) 1188–1196

Contents lists available at ScienceDirect

International Journal of Impact Engineering

journal homepage: www.elsevier.com/locate/ijimpeng

Analytical and experimental evaluation of energies during shock wave loading

Erheng Wang, Arun Shukla*

Dynamic Photomechanics Laboratory, Department of Mechanical, Industrial and Systems Engineering, The University of Rhode Island, Kingston, RI 02881, USA

ARTICLE INFO

Article history:
Received 24 August 2009
Received in revised form
28 June 2010
Accepted 27 July 2010
Available online 5 August 2010

Keywords:
Blast loading
Energy mitigation
Hugoniot relation
Shock tube

ABSTRACT

Analytical expressions were developed using gas dynamic equations to evaluate the energy associated with the incident shock wave (incident energy) and the reflected shock wave (remaining energy) for a shock tube experiment. The real time deformation profile of the specimen being loaded by a shock tube was also used to calculate the deformation energy. A shock wave loading on a homogeneous aluminum panel in a simple shock tube experiment was used to illustrate the implementation of these methods.

1. Introduction

The ability of a structure to absorb and reflect blast energy is extremely important in blast mitigation. Structures that can absorb and reflect blast energy effectively will efficiently dissipate and disperse the intensive pressure pulse and protect anything located behind them. Evaluating various energies, such as the energy stored in the shock wave and the energy transferred into the structures, will help in understanding the energy redistribution behavior during blast loading process; as a consequence the energy absorption and reflection properties of the structures can be evaluated.

However, the evaluation of energy contained in the blast wave and the transfer of this energy to the structure during a blast loading process is an important topic that is still not well understood. Taylor [1] first derived the relation between the blast overpressure and the energy released during an explosion. His pioneering work was utilized and extended in fluid-structure interaction theory [2,3]. Taylor [2] states that when the structures are exposed to the same blast, lighter structures acquire less momentum than heavier structures. The theoretical results from ref. [3] show that the energy transmitted to the structures can be reduced when the blast is applied to either very light structures or very heavy structures. However the fluid-structure interaction only occurs in a very short time period, when the blast wave (shock wave) impacts the structures [4,5]. After the shock wave impacts the structures, the gas located behind the wave front continues to load the structures. Therefore, these energies cannot be evaluated by the fluid-structure interaction theory alone.

The response of structures under blast loading has been widely studied. However, the results related to the energy absorption and dissipation are obtained through primarily numerical methods [6,7]. These numerical models were verified by the experimental deflection of the structures or their deformation modes. The numerical models were then used to calculate the energy absorbed or dissipated by the structures. Due to the difficulties that arise in regards to the measurement and calculation of energies for a real blast-loading event, these numerical results could not be verified.

Shock tubes have been widely used to study the dynamic behavior of structures under blast loading [8–10]. Due to the fact that a shock tube can generate a controllable shock wave with a planar wave front [11], it is possible to evaluate various energies by a shock tube experiment. In this research, the methods to evaluate the energies during a shock wave loading on a panel are proposed based upon the experimental data obtained from a shock tube experiment. The detailed steps to calculate the physical parameters of the gas, such as particle velocity, density and sound velocity of the gas, were described and implemented. The internal energy, the translational energy of the gases and the work done by the gases were evaluated using the calculated physical parameters. The total incident energy in the impinging gas, the total remaining energy in the gas after impact and the deformation energy of the specimen were also evaluated. A simple experiment on an aluminum panel using a shock tube was conducted to illustrate the implementation of these methods for evaluating energies.

* Corresponding author. Tel.: +1 401 874 2283.
E-mail address: shuklaa@egr.uri.edu (A. Shukla).

0734-743X/$ – see front matter © 2010 Elsevier Ltd. All rights reserved.
doi:10.1016/j.ijimpeng.2010.07.003

2. Theoretical consideration

A planar shock wave loading process generated by a shock tube experiment on a flat panel is used as a model to illustrate the evaluation methods of the energies. Fig. 1 shows a typical shock wave loading process. A planar incident shock wave front is traveling from the left side to the right side through a shock tube (incident process, Fig. 1a). The right side of the incident wave front is undisturbed gas, while the left side of incident wave front is the driver gas (helium) at a high pressure at the onset. After the incident shock wave impinges on a flat panel, which is located at the muzzle end of the shock tube, a reflected planar shock wave is then generated and travels from the right side to the left side (reflected process, Fig. 1b). The left side of the reflected wave front is still the driver gas, while the right side of the reflected wave front is now the gas that is disturbed by reflected shock wave. U_+ and U_- are the velocities of the incident and the reflected shock wave fronts, respectively. The state of the gas can be defined using the following physical parameters: p, the pressure; u, the particle velocity; c, the sound velocity; ρ, the density; τ, the specific volume (i.e. volume per unit mass); and e, the specific (internal) energy.

The subscript 0 on the parameters denotes the initial state of the gas. Subscript 1 represents the state of the gas located behind the incident shock wave front and it will be defined as the incident state. Subscript 2 represents the state of the gas located behind the reflected shock wave front and it will be defined as the reflected state.

2.1. Incident and remaining energies

The energy of a shock wave is stored in the gas, which is located behind the shock wave front. In the shock wave loading processes as shown in Fig. 1, there are two shock waves, the incident and the reflected shock wave. The energy stored in the gas located behind the incident shock wave front is defined as the incident energy and the energy stored in the gas located behind the reflected shock wave front is defined as the remaining energy.

The energy stored in the gas can be separated into three parts: the internal energy, the translational energy and the work done by the gas as it propagates through the cross-section of the shock tube.

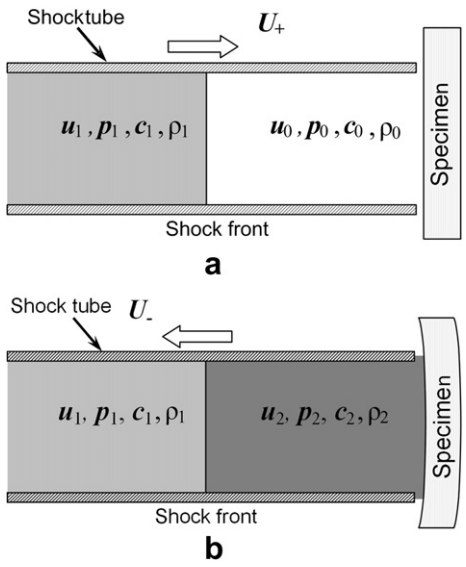

Fig. 1. Sketch of the incident and the reflected shock process. (a) Incident process. (b) Reflected process.

We assume that a gas with a pressure profile, $p(t)$, propagates within a shock tube with a cross-sectional area, S, with a particle velocity, $u(t)$. During time element dt, the internal energy of the gas [12], the translational energy and the work done by the gas can be described as following,

$$\mathrm{d}E_{\text{internal}} = \frac{p(t)^*S^*|u(t)|}{\gamma-1}\mathrm{d}t \tag{1}$$

$$\mathrm{d}E_{\text{translational}} = \frac{1}{2}^*(\rho(t)^*S^*|u(t)|)^*|u(t)|^2\mathrm{d}t = \frac{1}{2}\rho(t)^*S^*|u(t)|^3\mathrm{d}t \tag{2}$$

$$\mathrm{d}E_{\text{work}} = p(t)^*S^*|u(t)|\mathrm{d}t \tag{3}$$

where, γ is adiabatic exponent of the gas.

Therefore, the total energy stored in the gas can be obtained by integrating these energies with respect to time. The formulas for the incident energy E_{incident} and the remaining energy $E_{\text{remaining}}$ are as follows,

$$\begin{aligned} E_{\text{incident}} &= \int\left[\mathrm{d}E^{\text{incident}}_{\text{internal}} + \mathrm{d}E^{\text{incident}}_{\text{translational}} + \mathrm{d}E^{\text{incident}}_{\text{work}}\right] \\ &= \int S^*|u_1(t)|\left[\frac{\gamma^*p_1(t)}{\gamma-1} + \frac{1}{2}\rho_1(t)^*|u_1(t)|^2\right]\mathrm{d}t \end{aligned} \tag{4}$$

$$\begin{aligned} E_{\text{remaining}} &= \int\left[\mathrm{d}E^{\text{remaining}}_{\text{internal}} + \mathrm{d}E^{\text{remaining}}_{\text{translational}} + \mathrm{d}E^{\text{remaining}}_{\text{work}}\right] \\ &= \int S^*|u_2(t)|\left[\frac{\gamma^*p_2(t)}{\gamma-1} + \frac{1}{2}\rho_2(t)^*|u_2(t)|^2\right]\mathrm{d}t \end{aligned} \tag{5}$$

where, $p_1(t)$, $|u_1(t)|$ and $\rho_1(t)$ are, respectively, the incident pressure, the absolute value of particle velocity and the gas density behind the incident shock front, $p_2(t)$, $|u_2(t)|$ and $\rho_2(t)$ are the reflected pressure, the absolute value of particle velocity and the gas density behind the reflected shock front at any time, respectively.

In Eqs. (1)–(5), the cross-sectional area, S, of the shock tube is a known constant and the pressure profiles of the shock wave, $p(t)$, can be measured. The particle velocities of the gas, $|u(t)|$, the gas density, $\rho(t)$, and the sound velocities of the gas, $c(t)$, are unknown parameters and need to be calculated using experimental data and through the theory of gas-dynamics [12].

For polytropic gases, the physical parameters used to describe the state of gas have the following basic relationships,

$$\rho\tau = 1 \tag{6}$$

$$e = \frac{1}{\gamma-1}p\tau \tag{7}$$

$$\rho c^2 = \gamma p \tag{8}$$

$$p = A\rho^\gamma \tag{9}$$

where, A is a constant related to the initial state of the gas during a reversible adiabatic process (an isentropic process).

By following the basic laws of physics, the jump conditions for the shock wave can be derived and the procedure is shown below for the incident shock wave process (Fig. 1a) as an example:

$$\text{Conservation of mass}: \ \rho_0 v_0 = \rho_1 v_1 \tag{10}$$

$$\text{Conservation of momentum}: \ \rho_0 v_0^2 + p_0 = \rho_1 v_1^2 + p_1 \tag{11}$$

$$\text{Conservation of energy}: \frac{1}{2}v_0^2 + e_0 + p_0\tau_0 = \frac{1}{2}v_1^2 + e_1 + p_1\tau_1 \tag{12}$$

where, v is the relative particle velocity with respect to the shock wave front. $v_0 = u_0 - U_+$ and $v_1 = u_1 - U_+$.

Combining Eqs. (6), (10) and (11) gives,

$$(\tau_1 + \tau_0)(p_1 - p_0) = v_0^2 - v_1^2 \tag{13}$$

$$-\frac{p_0 - p_1}{\tau_0 - \tau_1} = \rho_0 v_0 = \rho_1 v_1 \tag{14}$$

$$\frac{p_1 - p_0}{\rho_1 - \rho_0} = v_0 v_1 \tag{15}$$

The Hugoniot relation can be derived by substituting Eq. (13) into Eq. (12),

$$H(\tau_1,\ p) = e_1 - e_0 + \frac{1}{2}(\tau_1 - \tau_0)(p_1 - p_0) = 0 \tag{16}$$

In the shock tube experiments, the parameters e and τ are extremely difficult to measure. Therefore, Eq. (16) needs to be modified into another form with different parameters, which are easier to obtain in experiments.

Substituting Eq. (7) into Eq. (16) gives,

$$\frac{p}{p} = \frac{\tau_0 - \mu^2\tau_1}{\tau_1 - \mu^2\tau_0} \tag{17}$$

Combining Eqs. (8), (14) and (17) gives,

$$\frac{p}{p} = \left(1 + \mu^2\right)M_0^2 - \mu^2 \tag{18a}$$

or,

$$\frac{p}{p} = \left(1 + \mu^2\right)M_1^2 - \mu^2 \tag{18b}$$

where, $\mu^2 = (\gamma - 1)/(\gamma + 1)$, and M is the Mach number, $M_1 = |u_1 - U_+|/c_1$ and $M_0 = |u_0 - U_+|/c_0$.

Finally, combining Eqs. (8), (12) and (15) gives,

$$\left(1 - \mu^2\right)(U_+ - u_0)^2 - (u_1 - u_0)(U_+ - u_0) = \left(1 - \mu^2\right)c_0^2 \tag{19a}$$

or,

$$\left(1 - \mu^2\right)(U_+ - u_1)^2 - (u_0 - u_1)(U_+ - u_1) = \left(1 - \mu^2\right)c_1^2 \tag{19b}$$

The jump conditions for the shock wave Eqs. (10)–(12) and the modified Hugoniot relations Eqs. (18) and (19) compose the system of governing equations. Only three equations in this system of equations are independent in the incident process (Fig. 1a). The same procedure can be applied to the reflected process (Fig. 1b) by changing the subscript 0 to 1, subscript 1 to 2 and subscript + to −. Thus, during a shock tube experiment, there are six independent equations. There are 15 parameters in the equations, p_0, p_1, p_2, u_0, u_1, u_2, c_0, c_1, c_2, ρ_0, ρ_1, ρ_2, U_+, U_- and γ. Note u_0 is zero, c_0 is the speed of sound in air, ρ_0 is the density of the air with one atmospheric pressure and room temperature, the adiabatic exponent, γ, is a gas constant and p_0, p_1, p_2, U_+, U_- can be measured. Therefore, there exist six unknown parameters, u_1, u_2, c_1, c_2, ρ_1 and ρ_2. These six unknown parameters can be determined using the six independent equations. Now, the incident and remaining energies can be calculated by substituting the value of physical parameters into Eqs. (1)–(5).

Note signs of the velocities in Eqs. (18) and (19) indicate the direction of motion. In Fig. 1, a positive sign indicates that the direction is the same as the propagating direction of the incident shock wave front and a negative sign indicates that the direction is opposite of the propagating direction of the incident shock wave front.

2.2. Deformation energy

After the incident shock wave impinges upon the panel, a reflected shock wave is generated and the reflected pressure is applied on the panel to deform the panel. The total work done by the gas to deform the panel is defined as deformation energy.

The calculation of the deformation energy requires the evaluation of the deflection–time data from the high-speed deflection images and the force-time data from the reflected pressure profile. Combining the deflection–time data and the force-time data will result in force–deflection data. Now, the deformation energy can be obtained by integrating the force–deflection data.

The deflection of the panel and the reflected pressure are two important quantities in the deformation energy calculation. Fig. 2 shows a typical real time side-view image of a deflected panel. Based on the experimental observation, the deflection of each point on a horizontal line along the width can be assumed to be the same. This means that the panel bends like a beam. Therefore, the deflection of the side view of the panel can be extended to the whole panel.

Since the force is applied on the front face of the specimen, the deflection of the front face of the specimen is what we need. Curve fitting methods, such as cubic spline curve fitting, polynomial curve fitting, etc., can be used to match the shape of the front face, as shown in Fig. 2. After calibrating the distance, the deflection of every point along the front face can be calculated.

By assuming that the pressure applied on the shock area is uniform and combining the pressure–time data and the deflection–time data, the pressure–deflection profile can be obtained. The deformation energy ($E_{\text{deformation}}$) can now be calculated by integrating the pressure–deflection profile for every point inside the shock loading area. The formula is as follows:

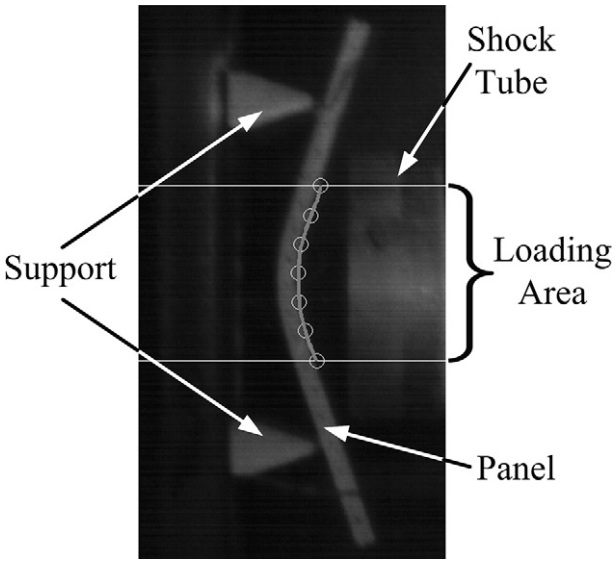

Fig. 2. Curve fitting to simulate the front face profile.

$$E_{\text{deformation}} = \oint_{S_{\text{shock tube}}} \left(\int p_2(t) \mathrm{d}l_{\text{deformation}} \right) \mathrm{d}S \tag{20}$$

3. Experimental procedure

A controlled shock wave loading experiment on a homogeneous aluminum panel was carried out using a shock tube to illustrate the implementation of the energy evaluation methods described above. The experimental setup is shown in Fig. 3. A shock tube apparatus was utilized to generate a planar shock wave with a controlled overpressure level. A flat aluminum panel was held in front of the end of the muzzle section. A high-speed digital camera, IMACON 200, was used to capture the real time side-view deformation images of the specimen. The detailed description of the shock tube apparatus can be found in Ref [8].

Detailed dimensions and locations of the muzzle, pressure transducers (PCB102A), specimen and supports are shown in Fig. 4. The inner diameter of the muzzle is 0.0762 m (3 in), which is also the diameter of the loading area. Two transducers are mounted at the end of the muzzle section to measure the incident pressure and the reflected pressure. The distance between the two transducers is 0.16 m and the distance between transducer 2 and the end of the muzzle is ~0.02 m.

The specimen panel was fabricated using 6061 Aluminum. The overall dimensions of the specimen are 101.6 mm (4 in) wide, 254 mm (10 in) long, and 10 mm (0.375 in) thick. The support fixtures ensure simply supported boundary conditions with a 0.1524 m (6 in) span and the support lines are parallel to the width of the panel.

In the present study, a shock wave, with an incident overpressure of approximately 1 MPa and a velocity of approximately 1045 m/s was generated and impacted on the panel. With an interframe time of 70 μs, 14 high-speed image frames of the loading process were obtained.

4. Experimental results

4.1. Velocity measurement of the shock wave fronts

The velocity of the shock wave fronts (U_+ and U_-) can be measured using the pressure profiles from the two transducers, which are shown in Fig. 4. Fig. 5 shows the typical pressure profiles from the two transducers.

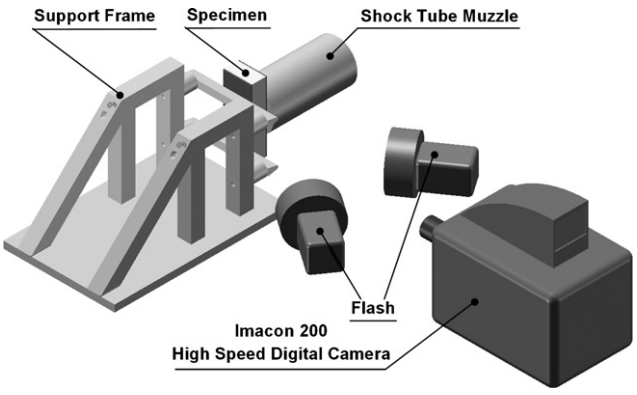

Fig. 3. Experimental setup.

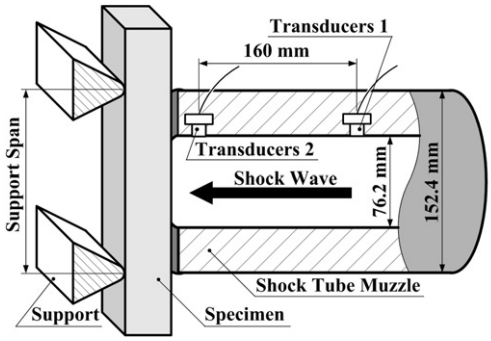

Fig. 4. Details of dimensions of the muzzle section.

An incident shock wave front travelling from left to right (Fig. 1a) through the muzzle section reached transducer 1 first, and gave a first jump on the pressure profile of transducer 1. This incident shock wave front then reached transducer 2 and gave a first jump on the pressure profile of transducer 2, as shown in Fig. 5. Thus, the time between the first jumps of two pressure profiles is the time taken by the incident shock wave to travel from transducer 1 to transducer 2. Since the distance between two transducers is known, the average velocity U_+ of the incident shock wave can be calculated. In present experiment, the time between the first jumps is 154 μs. Thus, the average velocity of incident shock wave is 1045 m/s.

Similarly, the reflected shock wave, generated after the incident shock wave impinges upon the panel, propagated in the opposite direction back down the barrel. Therefore, the reflected shock wave front reached transducer 2 first and subsequently reached transducer 1. The reach times are represented by the second jumps in the pressure profiles (Fig. 5). The average velocity U_- of the reflected shock wave can now be calculated using the distance between two transducers and the time between two second pressure jumps. In the present experiment, the time between two second pressure jumps is 444 μs. Thus, the average velocity of reflected shock wave is 363 m/s.

4.2. Incident and reflected pressure measurements

Since the pressure profiles were measured at the end of the muzzle section and not directly on the specimen, it is important to

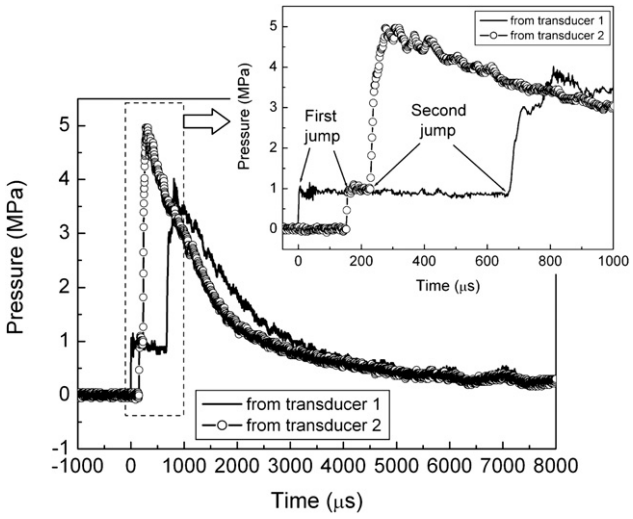

Fig. 5. Typical pressure profiles from two pressure sensors.

verify that both are indeed equal. A simple experimental setup, as shown in Fig. 6, was designed to verify this assumption. The two transducers were mounted at their original positions on the muzzle. A thick steel plate was placed in the same position as the test panel and supported firmly on the back side. An additional transducer, transducer 3, was mounted in the center of the loading area on the steel plate. Thus, the pressure profile from transducer 3 was exactly the pressure on the plate during the shock wave loading. Fig. 7 shows pressure profiles measured during the experiment from transducers 2 and 3. It is obvious that the measured pressure profile from transducer 2 is the same as the pressure profile exactly at the center of the plate.

Since the reflected pressure profile overlaps on the incident pressure profile (discussed in Section 4.1 and shown in Fig. 5), the pressure profiles obtained from the transducers cannot be used as pressure profiles of incident and reflected shock waves directly. The incident pressure profile can be acquired from the first to second jumps of the pressure profiles from two transducers. Due to the overlap problem, only 600–700 μs pressure profile can be used for energy evaluation. Total shock wave loading process lasts more than 5000 μs. Since the pressure pulses are repeatable in shock tube experiments [8,10], the incident pulse generated with the same initial overpressure was first recorded without the specimen in place. This pressure profile as shown in Fig. 8 was used in the calculation of the incident energy.

The reflected pressure profile was obtained from transducer 2 and is measured from the second pressure jump onwards. This is also shown in Fig. 8 and was used in the calculation of the remaining energy.

4.3. Calculation of the physical parameters

The incident and the reflected pressures in these experiments, as well as the gas particle velocities, the gas densities and sound velocities of the gas, are all functions of time. It is important to correlate the pressures and these physical parameters, which were used in the calculation of various energies. The calculation of the physical parameters can be separated into following steps.

4.3.1. Calculation of the initial values of the physical parameters ($t=0$)

The initial values of the physical parameters ($t=0$) at the time that the shock wave impinges on the specimen are significantly important for the calculation of the physical parameters at $t>0$. Though the process in which the gas crosses the shock wave front is an adiabatic process and not reversible, the other processes behind

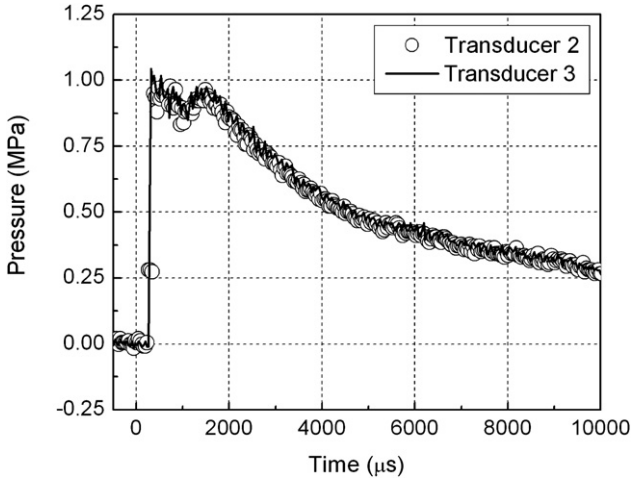

Fig. 7. Pressure profiles equality verification.

or in front of the shock wave front, such as the pressure change, are all reversible adiabatic processes (isentropic processes). Therefore, the values of the physical parameters at $t>0$ are all based on the initial values.

Based on the incident and reflected shock wave loading processes (shown in Fig. 1), three equations of the Hugoniot relations can be obtained using Eqs. (18) and (19).

$$(1-\mu^2)(U_+-u_0)^2-(u_{1\_\text{initial}}-u_0)(U_+-u_0) = (1-\mu^2)c_0^2 \tag{21a}$$

$$\frac{p_{2\_\text{initial}}}{p_{1\_\text{initial}}} = (1+\mu^2)\left(\frac{u_{1\_\text{initial}}-U_-}{c_{1\_\text{initial}}}\right)^2-\mu^2 \tag{21b}$$

$$(1-\mu^2)(U_--u_{1\_\text{initial}})^2-(u_{2\_\text{initial}}-u_{1\_\text{initial}})(U_--u_{1\_\text{initial}}) = (1-\mu^2)c_{1\_\text{initial}}^2 \tag{21c}$$

and another two equations can be obtained using Eq. (10),

$$\rho_0(u_0-U_+) = \rho_{1\_\text{initial}}(u_{1\_\text{initial}}-U_+) \tag{21d}$$

$$\rho_{1\_\text{initial}}(u_{1\_\text{initial}}-U_-) = \rho_{2\_\text{initial}}(u_{2\_\text{initial}}-U_-) \tag{21e}$$

where, p_{1_initial} and p_{2_initial} are the peak pressure values of the incident and reflected shock wave pressure profiles, respectively, U_+ and U_- were calculated from the experiment as described in

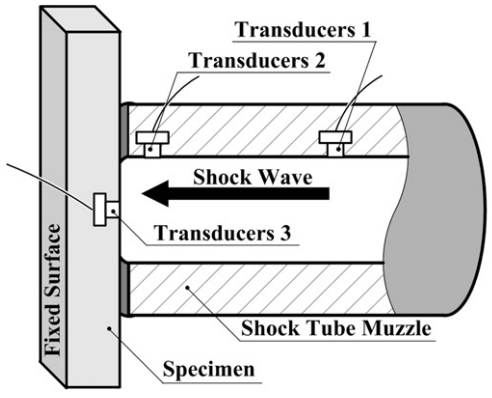

Fig. 6. Three pressure transducers setup.

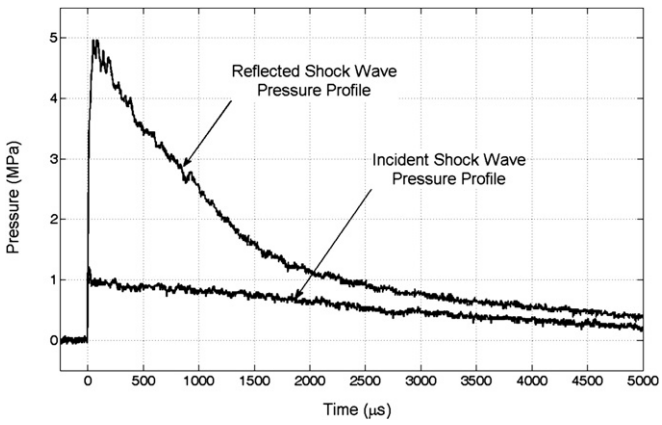

Fig. 8. Modified incident and reflected shock wave pressure profiles.

Section 4.1. $u_0 = 0$ m/s. $c_0 = 340$ m/s. $\mu^2 = (\gamma - 1)/(\gamma + 1)$ is the gas constant.

Thus, the initial value of the gas particle velocity behind the incident shock wave front can be explicitly derived from Eq. (21a) as,

$$u_{1\_\text{initial}} = u_0 + \frac{(1-\mu^2)(U_+ - u_0)^2 - (1-\mu^2)c_0^2}{U_+ - u_0} \tag{22}$$

The initial value of the sound velocity of the gas behind the incident shock wave front is derived from Eq. (21b),

$$c_{1\_\text{initial}} = |u_{1\_\text{initial}} - U_-| \sqrt{\frac{1+\mu^2}{(p_{2\_initial}/p) + \mu^2}} \tag{23}$$

The initial value of the gas particle velocity behind the reflected shock wave front is derived from Eq. (21c),

$$u_{2\_\text{initial}} = u_{1\_\text{initial}} + \frac{(1-\mu^2)(U_- - u_{1\_\text{initial}})^2 - (1-\mu^2)c_{1\_\text{initial}}^2}{U_- - u_{1\_\text{initial}}} \tag{24}$$

The initial value of the gas density behind the incident shock wave front is derived from Eq. (21d),

$$\rho_{1\_\text{initial}} = \left(\frac{u_0 - U_+}{u_{1\_\text{initial}} - U_+}\right)\rho_0 \tag{25}$$

The initial value of the gas density behind the reflected shock wave front is derived from Eq. (21e),

$$\rho_{2\_\text{initial}} = \left(\frac{u_{1\_\text{initial}} - U_-}{u_{2\_\text{initial}} - U_-}\right)\rho_{1\_\text{initial}} \tag{26}$$

In a shock tube experiment, prior to the diaphragm rupturing, one side of the diaphragm was filled with high-pressure helium (driver side), while the other side of the diaphragm was air (driven side) at normal pressure. After the diaphragm ruptured the compressive shock wave traveled from the direction of higher pressure to lower pressure (helium → air). Since the particle velocity of the helium gas located behind the shock front was less than the velocity of the shock front itself, airs passed over the shock front and occupied the space located between the helium gas and the shock front during the propagation of the shock wave. Therefore, by the time the shock wave reached the specimen, the gas located to the left and the right side of the shock front were both air. Thus, the adiabatic exponent of air, $\gamma = 1.4$, was used in present calculations.

4.3.2. Calculation of the densities and sound velocities of the gas at $t > 0$

Since the processes behind or in front of the shock wave front, such as pressure change and density change of the gas, are all reversible adiabatic processes (isentropic processes), the densities and sound velocities can be calculated using initial values and the state Eqs. (8) and (9) for a polytropic gas.

As a reminder, Eqs. (8) and (9) are as follows,

$$\rho c^2 = \gamma p \tag{8}$$

$$p = A\rho^\gamma \tag{9}$$

where, A is a constant related to the initial state of the gas during a reversible adiabatic process (isentropic process).

Through these two equations, the densities and sound velocities of the gas behind the incident shock wave front or in front of the reflected shock wave front at $t > 0$ can be calculated as,

$$\rho_1(t) = \left[\frac{p_1(t)}{p_{1\_\text{initial}}}\right]^{\frac{1}{\gamma}} \rho_{1\_\text{initial}} \tag{27a}$$

$$c_1(t) = \left[\frac{\rho_1(t)}{\rho_{1\_\text{initial}}}\right]^{\frac{\gamma-1}{2}} c_{1\_\text{initial}} \tag{27b}$$

The densities and sound velocities of the gas behind the reflected shock wave front at $t > 0$ are,

$$\rho_2(t) = \left[\frac{p_2(t)}{p_{2\_\text{initial}}}\right]^{\frac{1}{\gamma}} \rho_{2\_\text{initial}} \tag{28a}$$

$$c_2(t) = \left[\frac{\rho_2(t)}{\rho_{2\_\text{initial}}}\right]^{\frac{\gamma-1}{2}} c_{2\_\text{initial}} \tag{28b}$$

Figs. 9 and 10 show the calculated density and sound velocity change with respect to time.

4.3.3. Calculation of the particle velocities at $t > 0$

Before implementation of the calculation of the particle velocities at $t > 0$, two hypotheses are given as follows.

1. The velocity of reflected shock wave front does not change during the shock wave loading process.
2. The physical properties of the gas, such as pressure and particle velocity, located on each side of the reflected shock wave front are uniform.

Then the particle velocities can be calculated by the analysis described below.

Based on the reflected process (shown in Fig. 1b), two equations using different forms of the Hugoniot relation can be obtained.

$$\frac{p_2(t)}{p_1(t)} = \left(1+\mu^2\right)\left(\frac{u_1(t) - U_-}{c_1}\right)^2 - \mu^2 \tag{29a}$$

$$\left(1-\mu^2\right)[U_- - u_1(t)]^2 - [u_2(t) - u_1(t)][U_- - u_1(t)] = \left(1-\mu^2\right)c_1^2 \tag{29b}$$

In these two equations, the first hypothesis allows one to use the average reflected shock wave velocity described in Section 4.1. The second hypothesis allows one to use the measured pressure profile

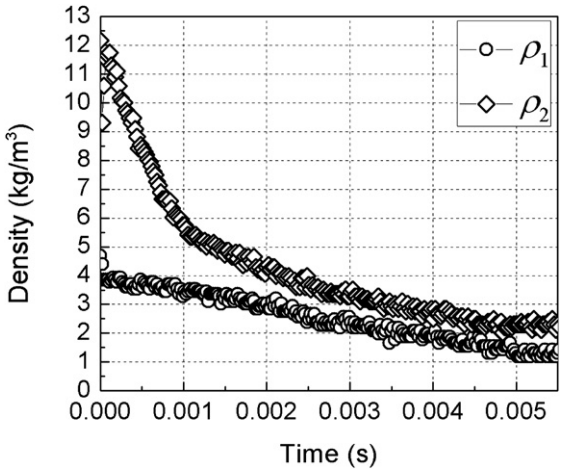

Fig. 9. Density change.

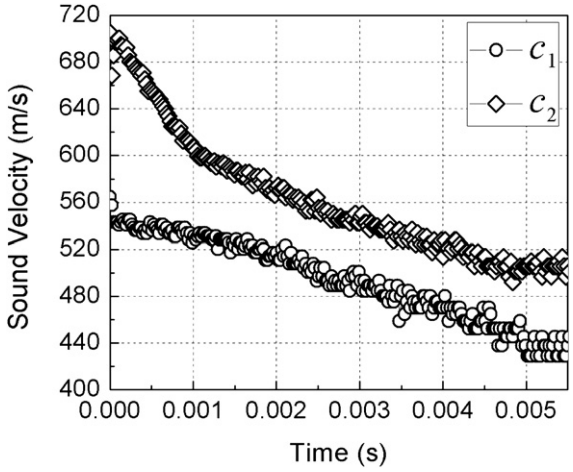

Fig. 10. Sound velocity change.

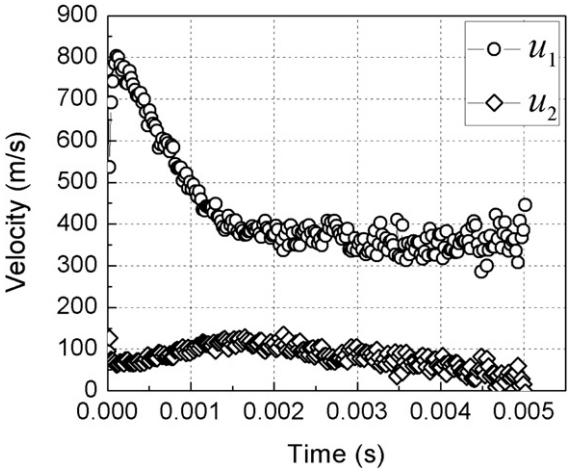

Fig. 11. The comparison of the particle velocities.

at the muzzle to replace the pressure data in Eq. (29), which denotes the pressure exactly located in front of and behind the reflected shock wave front, though the reflected shock wave front is propagating.

Therefore, the particle velocities of the gas located on both sides of the reflected shock wave front can be solved as,

$$u_1(t) = U_- + c_1\sqrt{\frac{[p_2(t)/p_1(t)]+\mu^2}{1+\mu^2}} \tag{30a}$$

$$u_2(t) = \frac{(1-\mu^2)\left\{[U_- - u_1(t)]^2 - c_1^2\right\}}{U_- - u_1(t)} + u_1(t) \tag{30b}$$

where, $p_1(t)$ and $p_2(t)$ were the incident and reflected shock wave pressure profiles, which were shown in Fig. 8.Eqs. (30a) and (30b) were substituted into Eqs. (1)–(5) and subsequently Eqs. (4) and (5) were numerically integrated to obtain the incident and the remaining energies. Fig. 11 shows the comparison of u_1 and u_2 for the present experiment.

4.4. Side view deflection reconstruction

Real time side view images of the panel deflection are shown in Fig. 12. Seven points were chosen along the profile of the front face of the panel in each image, as shown in Fig. 2. The spline curve fitting method was utilized to track the deformation of the front

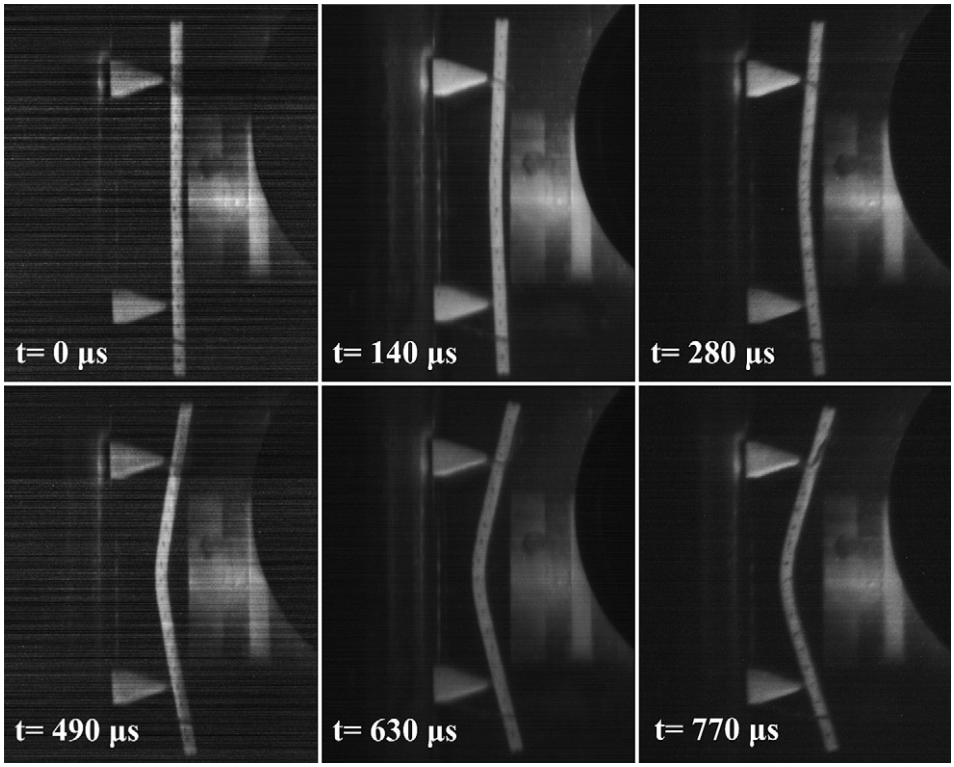

Fig. 12. High-speed deflection images.

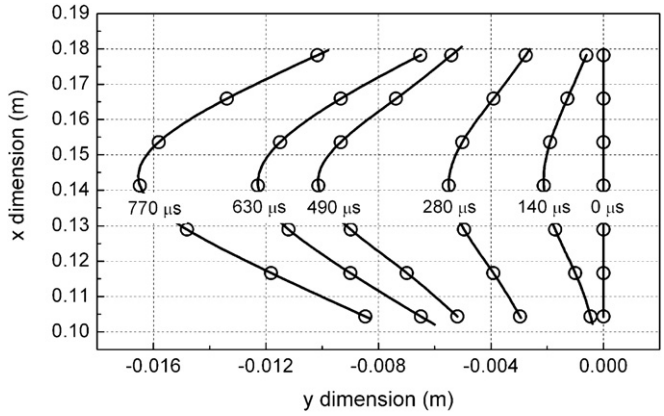

Fig. 13. Reconstructed shape of the panel at different time.

face. The reconstructed shapes along with the seven data points used are shown at six time intervals in Fig. 13. Since the pressure was applied to the panel within the muzzle's inner cross-sectional area, the reconstruction was only carried out for this area. Through this reconstruction, the deflection data of each point on the front surface of the panel (such as Fig. 2) can be obtained and utilized in the calculation of the deformation energy.

4.5. Energy evaluation

The internal energy, the translational energy and the work done by the gas obtained from Eqs. (1)–(3) are shown in Fig. 14. It can be seen that the highest energy is the incident internal energy of the impinging gas. The incident translational energy is about 1/3 of the incident internal energy and the work done by the incident gas is about 1/4 of the incident internal energy. After the shock wave loading on the specimen, the levels of the remaining energies were highly reduced. The remaining internal energy is only 2/5 of the incident internal energy. The work done by the reflected gas is about 1/5 of the incident internal energy and the remaining translational energy is almost zero. This is due to the substantially lower reflected gas particle velocity, which is roughly less than 20% of the incident gas particle velocity.

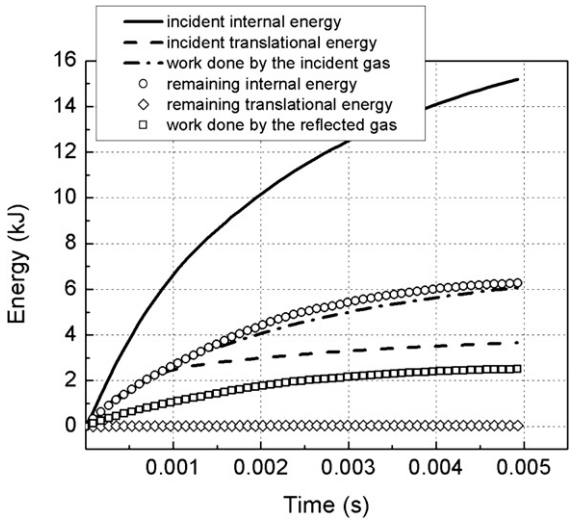

Fig. 14. Evaluated energies of different types.

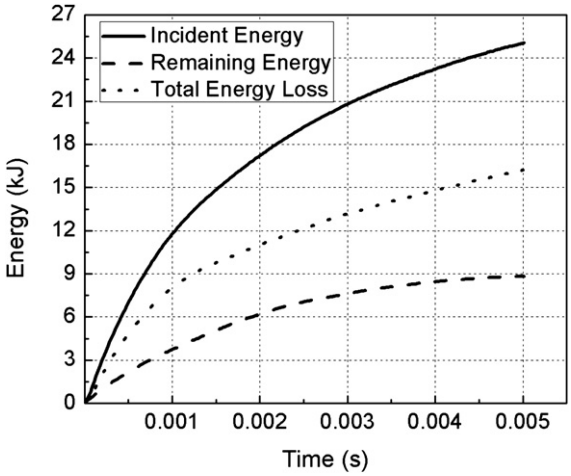

Fig. 15. The incident energy, remaining energy and total energy loss.

The total incident and remaining energies obtained from Eqs. (4) and (5) are shown in Fig. 15. It can be seen that the incident energy is much larger than the remaining energy, which indicates that there is a large amount of the energy lost during the shock wave loading process. The energy difference between the incident and remaining energy is termed as the total energy loss. This total energy loss is consumed in panel deformation energy, panel kinetic energy, heat, sound, light and any energy lost out of the side of the panel.

The deformation energy was calculated by substituting the modified reflected pressure profile in Fig. 8 and the reconstructed deformation information in Section 4.4 into Eq. (20). The evaluated deformation energy is shown in Fig. 16. Since the high-speed images captured by the camera covered about 1 ms, the deflection energy was only calculated for this time duration. From Fig. 16, it can be seen that a very small amount of energy, which is less than 5% of the total incident energy, is used to deform the panel and the bulk of the energy is lost elsewhere.

4.6. Discussion of the errors from the hypotheses

In Section 4.3.3, we have given two hypotheses in order to implement the calculation process of the particle velocities. They will induce some errors in the calculations. In this section, we discuss the feasibility of these hypotheses.

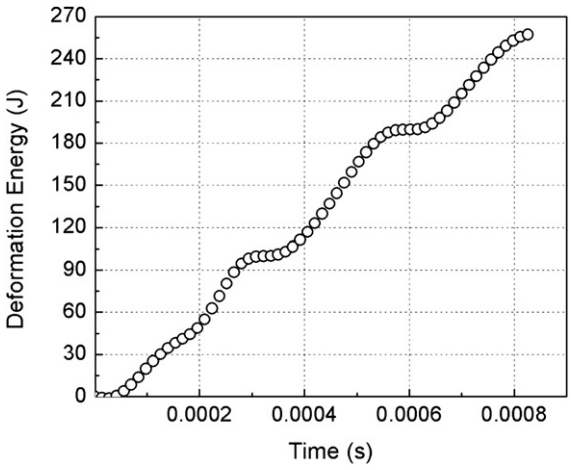

Fig. 16. The deformation energy.

For the first hypothesis, the average velocity of the reflected shock wave front used in this study is 363 m/s. This average velocity is close to the speed of sound (340 m/s) in the air with one atmospheric pressure and room temperature. As we know, the weak shock wave will propagate with the speed of sound of the gas. The average velocity of the reflected shock wave front will only change less than 10% of its original value. Therefore we can conclude that the first hypothesis is feasible.

For the second hypothesis, the synchronized pressure profiles, which were measured from the different locations on the muzzle and shown in Fig. 5, can be utilized to verify this hypothesis. Two time periods need to be considered. The first time period is between the time that the incident shock wave reached transducer 2 (correlate to the first jump of the pressure data from transducer 2) and the time that the reflected shock wave reached transducer 2 (correlate to the second jump of the pressure data from transducer 2). During this time period, two transducers measured the pressure data of the gas located behind the incident shock wave front, which correlates to the state 1 in Fig. 1. The second time period is after the reflected shock wave reached transducer 1 (correlate to the second jump of the pressure data from transducer 1). During this time period, two transducers measured the pressure data of the gas located behind the reflected shock wave front, which correlates to the state 2 in Fig. 1. It can be seen that the pressure profiles overlapped very well during the first time period. This indicates that the physical parameters behind the incident shock wave are uniform. During the second time period, the pressure profiles from two transducers overlapped during a majority of the time (over 60% of the total time) of the shock wave loading process. The region where there was no overlapping of pressure profiles within the second time period, the difference between them is less than 15%. Thus, it can be concluded that the second hypothesis is also feasible.

5. Summary

In this study, the method to evaluate the energies associated with the incident shock wave, the reflected shock wave and the energy that deforms the specimen in a shock tube experiment have been developed. The determination of these energies is based on the shock wave pressure profiles and the high-speed deformation images that are obtained during a shock tube experiment. The implementation of this method is demonstrated by conducting a controlled experiment on a homogeneous aluminum panel using a shock tube. The results indicate that only a small amount of the incident energy was used in deforming the specimen and imparting kinetic energy to the specimen. Most of the incident energy remained in the gas and was dispersed as heat, sound, light and other forms of the energy and losses through the sides of the panel.

Acknowledgements

The authors kindly acknowledge the financial support of the Office of Naval Research (Dr. Y.D.S. Rajapakse) under grant no. N000140410268, and of the Department of Homeland Security under Cooperative Agreement No. 2008-ST-061-ED0002.

References

[1] Taylor GI. The formation of a blast wave by a very intensive explosion. I. Theoretical discussion. Proc Roy Soc A 1950;201:159–74.
[2] Taylor GI. The pressure and impulse of submarine explosion waves on plates. In: Batchelor GK, editor. Aerodynamics and the mechanics of projectiles and explosions. The Scientific Papers of Sir Geoffrey Ingram Taylor, vol. III. Cambridge University Press; 1963. p. 287–303.
[3] Kambouchev N. Analysis of blast mitigation strategies exploiting fluid–structure interaction. PhD dissertation, Massachusetts Institute of Technology; 2007.
[4] Xue Z, Hutchinson JW. A comparative study of impulse-resistant metal sandwich plates. Int J Impact Eng 2004;30:1283–305.
[5] Qui X, Deshpande VS, Fleck NA. Dynamic response of a clamped circular sandwich plate subject to shock loading. J Appl Mech 2004;71:637–45.
[6] Netmat-Nasser S, Kang WJ, McGee JD, Guo WG, Isaacs JB. Experimental investigation of energy-absorption characteristics of components of sandwich structures. Int J Impact Eng 2007;34:1119–46.
[7] Zhu F, Zhao L, Lu G, Wang Z. Structural response and energy absorption of sandwich panels with an aluminium foam core under blast loading. Adv Struct Eng 2008;11:525–36.
[8] LeBlanc J, Shukla A, Rousseau C, Bogdanovich A. Shock loading of three-dimensional woven composite materials. Compos Struct 2007;79:344–55.
[9] Tekalur SA, Shukla A, Shivakumar K. Blast resistance of polyurea based layered composite materials. Compos Struct 2008;84:271–81.
[10] Wang E, Gardner N, Shukla A. The blast resistance of sandwich composites with stepwise graded cores. Int J Solid Struct 2009;46:3492–502.
[11] Stoffel M, Schmidt R, Weichert D. Shock wave-loaded plates. Int J Solid Struct 2001;38:7659–80.
[12] Courant R, Friedrichs KO. Supersonic flow and shock waves. New York: Interscience Publishers; 1948.